Photonic crystals with rainbow colors by centrifugation-assisted assembly of colloidal lig-nin nanoparticles

Jinrong Liu
Stockholm University
Mathias Nero
Stockholm University https://orcid.org/0000-0003-2574-3655
Kjell Jansson
Stockholm University
Tom Wilhammar
Stockholm University
Mika Sipponen (mika.sipponen@mmk.su.se)
Stockholm University https://orcid.org/0000-0001-7747-9310

Article

Keywords:

Posted Date: December 14th, 2022

DOI: https://doi.org/10.21203/rs.3.rs-2339485/v1

Additional Declarations: There is **NO** Competing Interest.

Version of Record: A version of this preprint was published at Nature Communications on May 29th, 2023. See the published version at https://doi.org/10.1038/s41467-023-38819-5.

Photonic crystals with rainbow colors by centrifugation-assisted assembly of colloidal lignin nanoparticles

*Jinrong Liu, Mathias Nero, Kjell Jansson, Tom Willhammar, Mika H. Sipponen**

Department of Materials and Environmental Chemistry, Stockholm University, Sweden

**Corresponding author: mika.sipponen@mmk.su.se*

Abstract

Photonic crystals are optical materials that are often fabricated by assembly of particles into periodically arranged structures. However, assembly of lignin nanoparticles (LNPs) into close-packed structures has been limited due to lacking methods and incomplete understanding of the interparticle forces and packing mechanisms. Here we show a centrifugation-assisted fabrication of photonic crystals by classifying LNPs according to their particle size. Regardless of the initial broad size distribution of LNPs, centrifugation produced monodispersed particle layers that displayed gradient colors from red to violet in agreement with their size distribution and reflectance spectra. Each assembled layer of LNPs displayed semi-closed packing structures, which gave rise to coherent scattering and the resulting rainbow structural colors. *In situ* optical microscope images provided additional evidence on the importance of dynamic rearrangement of LNPs during their assemble into semi-closed packed structures. The preparation of LNPs combined with the methodology for their classification and assembly pave the way for a new generation of sustainable photonic crystals.

Introduction

Shimmering colors have fascinated people throughout the recorded history of humankind[1,2]. Many of the natural colors are structural colors originating from scattering and diffraction of close-packed particles such as silica in opal[3,4]. More specifically, the periodic structure of a photonic crystal allows specific electromagnetic waves to propagate and specific ones to be forbidden, which gives rise to a photonic band gap[5]. Visible coloration results when the lattice constant (the lengths a, b, and c of the

three cell edges meeting at a vertex, and the angles α, β, and γ between those edges) of the crystal is comparable or smaller than the wavelength of light and the bandgap corresponds to a wavelength in the visible range (400−800 nm).

Artificial photonic crystals can be produced by self-assembly of monodisperse particles[6–8]. The assembly process can be manipulated by various external forces, such as gravitational or inertial forces[6], surface tension or capillary forces[9,10], or electric or magnetic fields[11]. A vast majority of these artificial photonic crystals are assembled from colloidal silica[7,12] or polymer spheres (frequently polystyrene or polymethyl methacrylate)[13,14]. However, the aforementioned particles have obvious shortcomings stemming from their sources, production and end-of-life management. There is thus a growing demand for photonic materials based on renewable biomass.

Lignin as the second most abundant component of wood and the main by-product of the pulping industry is an important biomass resource[15]. It is an aromatic heteropolymer with mostly dark-brownish color which originates from its intrinsic chromophores and those formed during the pulping reactions[16]. The brown-black color palette of industrial lignin limits the opportunity window for applications[17]. Lignin-retaining bleaching to remove the chromophores is not a fully sustainable strategy due to the dearomatization reactions and generation of degradation products[18].

Structural colors based on lignin could be a way forward as the amphiphilic nature of lignin makes it plausible to form spherical lignin nanoparticles (LNPs) by aggregation in aqueous solvents[19,20]. Lignin fractionation is developed to engineer lignin into a value-added material[21–24]. In addition to their renewable origin, one advantage of LNPs is their charge stabilization due to carboxylic and phenolic hydroxyl groups[25], which therefore permits avoiding the use of a surfactant. However, LNPs are not well studied in preparing photonic crystals because of insufficient understanding of their packing mechanism. In addition, one strict requirement in preparation of photonics is to have narrow particle size distribution (<5%) for achieving close-packed structures. LNPs do not naturally qualify for this requirement due to their polydispersity. In this sense, Wang et al.[26] managed to fabricate monodispersed LNPs by a solvent extraction method. Such monodispersed particles could form different color tones in powder form.

Here we show that lignin photonic crystals with rainbow coloration can be prepared from non-monodispersed LNPs. The rainbow-colored crystals in the size range from 1 mm to 1 cm are produced by centrifugation of LNPs based on commercial soda lignin. Our results show that centrifugation is central to achieving distinct layers of monodispersed LNPs. These results represent a major step towards lignin-based structural colors and tailormade photonic materials.

Results

The first question relevant to photonic crystals that we need to answer is which size distribution is proper for lignin-based materials. To answer this question, we can look into origin of this phenomenon. Structural colors are observed when electromagnetic waves are Bragg-scattered in certain directions owing to a high extent of spatial periodicity in the particle lattice[27]. Therefore, the particle size which responds to different visible wavelength scales (at normal incidence) can be predicted from the diffraction of electromagnetic waves following a modified Bragg's law[7,28,29]. The calculated particle diameter range that matches the colors from violet to red is from 158 to 311 nm (Table 1). In other words, when the particle size decreases, the photonic band gap exhibits a blue-shift.

Table 1. Calculation of particle size of the structural color based on Bragg's law.

	Violet	Blue	Green	Yellow	Orange	Red
λ (nm)	380−450	450−495	495−570	570−590	590−620	620−750
D (nm)	158−187	187−205	205−236	236−245	245−257	257−311

Based on the data in Table 1 we prepared LNPs with a size distribution that we anticipated to be suitable for the formation of structural colors by centrifugation-assisted assembly of LNPs. The procedure how to prepare LNPs and photonic crystals is shown in Fig. 1. In our case the starting material was soda lignin that was purified by successive solvent extractions first with ethanol and the remaining solids with acetone, following a procedure reported in the literature[26]. The resulting acetone-soluble fraction comprised around 10% of the original soda lignin and was used to prepare LNPs by a solvent shifting

method[30]. The prepared LNPs showed an average hydrodynamic diameter of 184 nm (Fig. 2a) and a polydispersity index (PDI) of 0.19 based on dynamic light scattering (DLS). The theoretical range (158 nm to 311 nm) over which LNPs can generate partial photonic band gaps from violet to red is marked by a rainbow color background in Fig. 2a. The hydrodynamic size can be adjusted by varying the water dilution rate during the solvent shifting method, from 184 to 582 nm, rate from 20 to 0.25 v/v/min (SI Fig. S1). The smallest particles (184 nm) were achieved by the fastest water dilution rate (20 v/v/min), which follows the reported trend in literature[19]. The concentration of the as-prepared dispersion of LNPs was 0.18 wt%. This dispersion was centrifuged to separate small particles which were out of range with respect to the predicted contribution to the photonic band gap. The remaining part of the centrifuged LNPs was classified into different layers in the pellet according to their particle size. By DLS we confirmed that each layer of the centrifuged LNPs has a narrow PDI (<0.05), which is important for their close-packing.

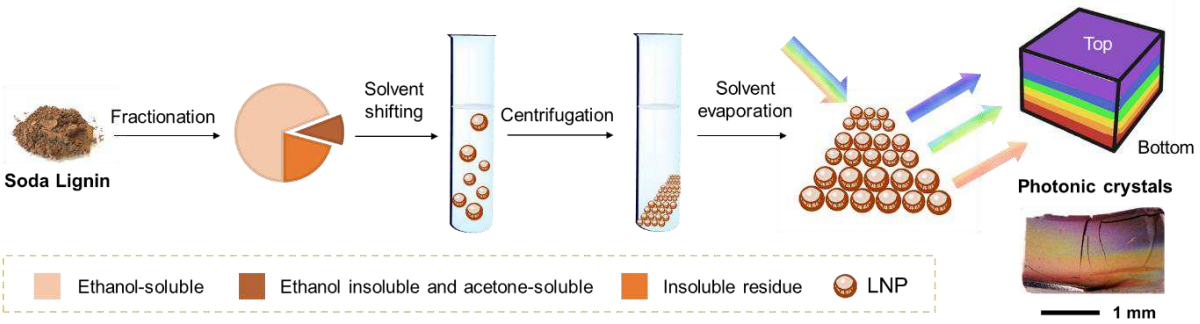

Figure 1. Scheme of preparation of photonic crystals from lignin. Solvent fractionation of soda lignin and preparation LNPs by a solvent shifting method. After centrifugation, the layers of the rainbow-colored crystal form according to the particle diameter. Bottom right: Digital microscope image of a photonic crystal from LNPs.

We observed a red to violet rainbow coloration across the cross-section of the crystal collected from the pellet, with violet color on the surface. This coloration remained stable after drying of the pellet under ambient temperature, as shown in Fig.1 with a microscope image. These results indicate that LNPs interact with light because the spacings of the ordered regions of LNPs fall within the wavelength region of visible light.

Crystallization from colloidal dispersion to crystal phases has been observed when increasing the particle concentration[13] for example by gravitational sedimentation[7] or vertical deposition[6]. However, materials with a photonic band gap do not always form spontaneously upon reaching a threshold concentration in the colloidal dispersion[31]. For example, when we let a dispersion of LNPs evaporate in a Petri dish at room temperature, we observed formation of rectangular platelets (Fig. 2b-c). Although such ordered platelet patterns were formed by evaporation-induced self-assembly no structural color was observed (Fig. 2b). Due to the absence of a photonic band gap the platelets remained brownish in accordance with the original lignin color. A higher magnification SEM image of the surface of a single platelet revealed that it consists of rather polydisperse distribution of particles (Fig. 2e). In addition to showing some unfilled spots within the surface the average size of LNPs was 77 nm, with standard deviation of 20 nm, and PDI of 0.07 (SI Fig. S2). In addition to the PDI exceeding 0.05 the particle size was below that predicted to form structural colors (Table 1). Nevertheless, the ordered rectangular structure provided first hints towards the ability of LNPs to assemble into close-packed domains and suggest that the process may require size-dependent sedimentation and particle classification.

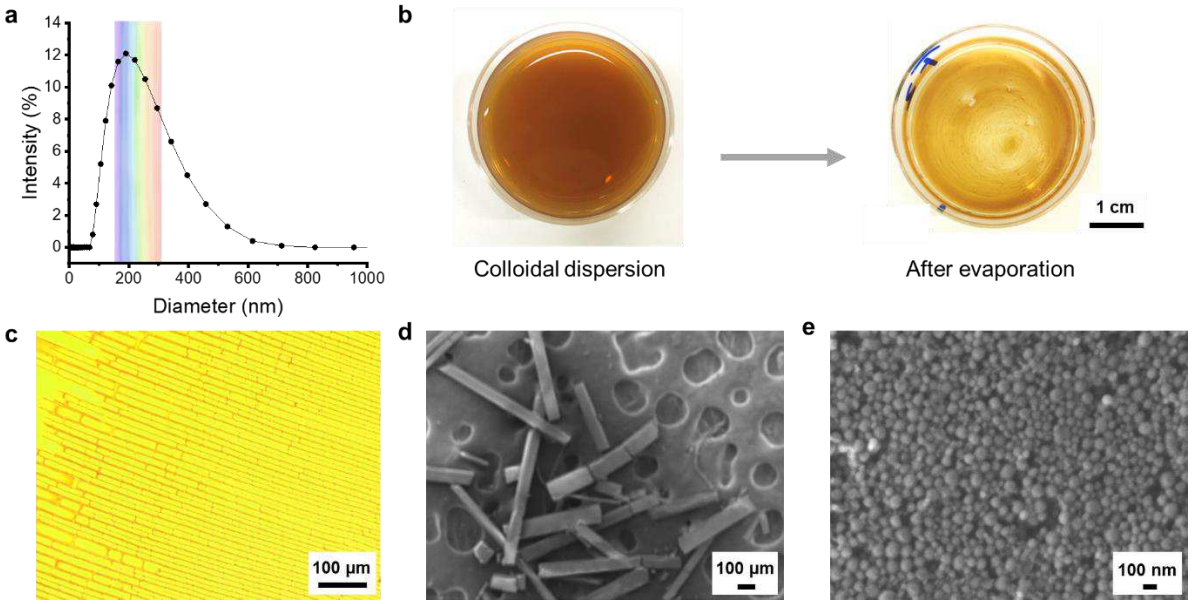

Figure 2. Formation of strip pattern of LNPs by evaporation-induced self-assembly. (a) Size distribution of LNPs based on DLS. (b) Digital photos of Petri dish before and after evaporation. (c) Optical microscope image of strip patterns. (d) and (e) SEM images of platelets and a closer view of a single platelet surface.

Since evaporation-induced self-assembly only works in forming platelet patterns, we hypothesized that centrifugation of LNPs could assist the formation of photonic materials. There are two important effects that centrifugation may have on the formation of ordered close-packed structures. Firstly, centrifugation provides a rapid way to increase the volume fraction of LNPs. This is important from theoretical foundation point of view that considers that the threshold volume fraction needs to be overcome to achieve phase transition is 0.494[13]. Secondly, centrifugation classifies LNPs based on their hydrodynamic diameter, which is important for achieving monodisperse subdistributions. After centrifugation, we observed a brownish supernatant and a colorful pellet in wet state (Fig. 3a, left digital photo). The brownish color of the supernatant comes from small LNPs which did not sediment. Violet is the main color on the surface of the pellet, while also some blue and green coloration can be observed on the edges. We removed the supernatant and dried the pellet at room temperature. We observed gradient colors after complete solvent evaporation (Fig. 3a, right digital microscope image), which means good stability of the photonic structure. The violet color was on the top surface of the dried pellet and the red color is on the bottom surface. In between, we observed a rainbow-type color gradient. The order of the colored layers matches that of the predicted particle size ranges (Table 1). The red layer was on the bottom because it originates from the largest particles in the population, and sediment first during the centrifugation. In turn, small particles are on the top because they have a slower rate of sedimentation and thus contribute to the violet photonic band gap.

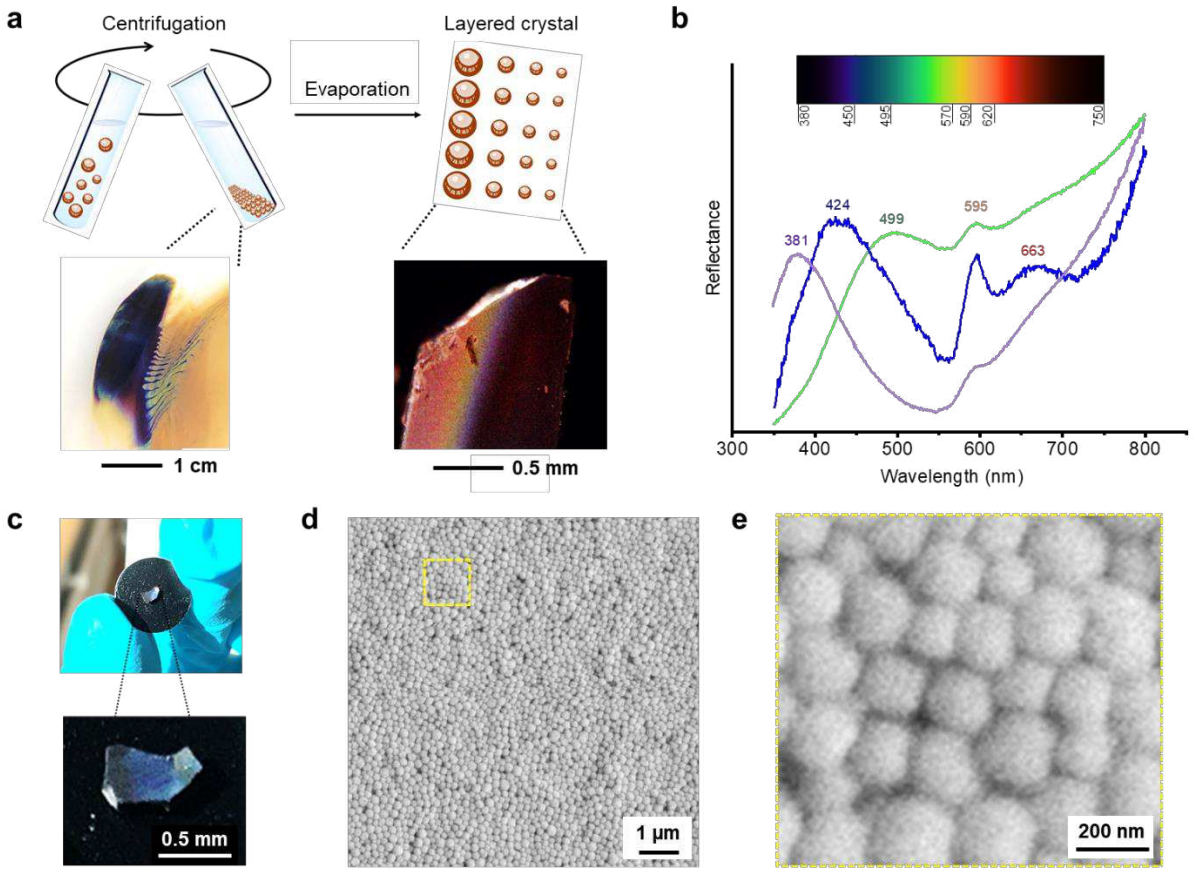

Figure 3. Centrifugation-assisted formation of photonic crystal from LNPs and characterization of the optical and structure properties. (a) Scheme of forming photonic crystal from LNPs by centrifugation. Digital photo of the pellet after centrifugation (left) and digital microscope image of cross-section of LNPs photonic crystal (right). (b) Reflectance spectra (c) Digital photographs and (d) and (e) SEM images of the photonic crystals.

In agreement with our visual observations, UV-vis reflection spectra revealed peaks in various wavelength regions of visible light. The peaks at 381 nm 424 nm 499 nm 595 nm, 663 nm are responsible for violet, blue, green, orange, and red respectively (Fig. 3b). The yellow peak is unclear, which might be because yellow light has the narrowest wavelength range (570–590 nm) and correspondingly only a low amount of LNPs fell to the corresponding particle size range (236–245 nm, Table 1). Another reason might be the strong adjacent peaks from orange and green colors. A digital photograph in Fig. 3c shows a fragment of blue LNPs photonic crystal. The structural color originates from coherent scattering of light within the ordered photonic structures[27]. This ordered structure was

revealed by microscopic imaging by SEM. As shown in Fig. 3d, some ranges of LNPs are semi-hexagonally close-packed. The periodic structure allows the diffraction of white light.

The size-dependent structure color of the photonic crystals was predicted by theoretically calculated particle diameters of LNPs (Table 1). Here we further confirm the trend of size-dependence by SEM imaging and compare the experimental results with the theoretical values. To image samples with SEM, we sputter coated the surfaces of the samples with gold, which did not change their color as observed color appearance (SI Fig. S3). As shown in Fig. 4a, the cross-section of LNPs photonic crystal exhibits a gradient color from violet to red. By imaging different color layers across the photonic crystal, we collected corresponding SEM images, as shown in Fig. 4, (c) in violet, (d) in blue, (e) in green, (f) in yellow, (g) in orange, and (h) in red. The size distributions of LNPs in each color layer were more uniform and monodispersed than in Fig. 2e which is the image of LNPs after gravitational sedimentation. Image analysis of the SEM micrographs gave the size distributions of LNPs in different layers (Fig. 4b). The peaks of particle size distributions were located at 150, 160, 170, 180, 200, and 240 nm, from (a) to (f) respectively. The size-dependence of LNPs photonic crystal agrees with the photonic theory, that is, a reduction in size induce a blue-shift when the refractive index and packing structure remain constant. The range of particle diameter of LNPs for different colors acquired from SEM images is narrower than the predicted in Table 1. This might be because, despite their structural color, LNPs were not perfectly close-packed in cubic domain therefore the real inter planar spacing d_{111} might be slightly higher than predicted from equation (2).

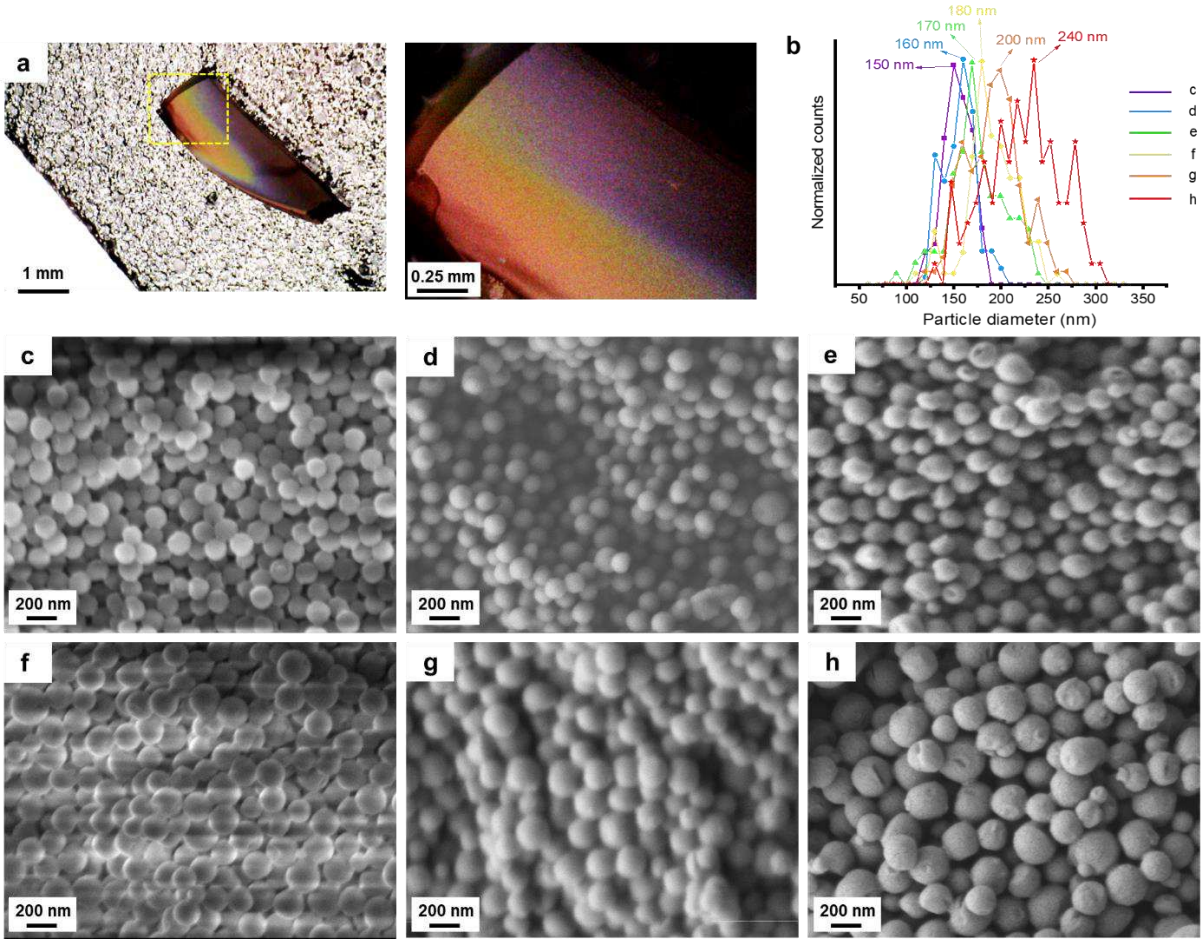

Figure 4. Characterization of the structure of LNPs photonic crystal at different color layers. (a) Digital microscope image of cross-section of a photonic crystal. (b) Size distributions of LNPs in different color layers of the photonic crystal. More than 100 particles were measured in SEM images (c – h). The peaks are at 150 nm, 160 nm, 170 nm, 180 nm, 200 nm, and 240 nm respectively. (c) – (h) SEM images of LNPs in different color layers (from violet to red) of the photonic crystal.

To reveal more insight into the packing of LNPs inside the crystals, we sectioned the photonic crystal by ultramicrotomy. SEM image of the block face and scanning transmission electron microscope (STEM) image of a 200 nm thick section from the LNPs photonic crystal reveal its internal structure and to prove that monodisperse packing occurred across the crystal (SI Fig. S4). After these insights we transferred our attention to elucidate the mechanism by which LNPs form ordered photonic structures.

Narrow size distribution is considered important in forming colloidal crystals[32]. In line with this foundation, we found that PDI of LNPs in all layers of the photonic crystals were lower than 0.05. As

shown in Fig. 5a, calculated from the size distributions in Fig. 4b, the PDIs of the layers corresponding to red to violet colors were between 0.008-0.043, which is markedly lower than the PDI of initial LNPs (0.07, SI Fig. S2). The monodispersity increased by centrifugation is important to the formation of photonic crystal. We see in Fig. 5b that centrifugation can separate LNPs in supernatant and pellet according to size, 70 nm and 190 nm, PDI 0.08 and 0.18, respectively. Theoretically, particles with a diameter of 70 nm are too small to generate a photonic band gap (Table 1). Therefore, removing the supernatant enriched with the smaller particles helps to avoid formation of defects in the photonic crystals.

The size separation in the process of centrifugation can be studied by varying centrifugation force and time. Based on Stoke's law, the velocity (v) of sedimentation can be calculated from: $v = \frac{D^2(\rho_{Particle} - \rho_{Liquid}) \times g}{18\mu}$, therefore the velocity depends on five parameters. When the density of particles ($\rho_{Particle}$), density of liquid (ρ_{Liquid}), gravitational force (g), and solvent viscosity (μ) are constant, particles size (D) is crucial to the sedimentation speed, which can be proved by differential centrifugation experiments. As shown in Fig. 5d, the initial hydrodynamic size of LNP was 183 nm, PDI 0.19. After centrifugation with RCF of 600 *g*, the particle diameter in the supernatant decreased to 146 nm, which means that large particles in the initial dispersion participated in the formation of the pellet. Then the supernatant was centrifuged in a second run with RCF of 2000 *g*, and the second supernatant showed a diameter of 129 nm. After the third run of centrifugation with RCF 3800 *g*, the particle diameter in the supernatant slightly decreases to 114 nm. We can conclude that bigger particles have a faster rate of precipitation; to allow smaller particles to participate in the sedimented phase higher RCF is needed. The influence of centrifugation time is shown in Fig. 5f by carrying out several parallel experiments. Here we chose LNPs with larger hydrodynamic size ~300 nm and broader PDI of 0.28 (SI Fig. S1) to demonstrate the time influence of centrifugation. As shown in Fig. 5f, the average particle diameter in the supernatant decreases when longer centrifugation time is applied. After short centrifugation time of 15 s, no significant change was observed in the size distribution. After 180 s centrifugation, the particle size in the supernatant decreased to 285 nm, which means that large particles in the initial dispersion formed the pellet. The particle size decreased to 263 nm after 300 s and further

to 244 nm after 360 s of centrifugation, which means that both large and medium-sized particles were deposited to the pellet. As shown in the illustration of Fig. 5e, after centrifugation for 360 s, the size gradient from large to small occurs from bottom to top in the pellet, which corresponds to the SEM results in Fig. 4. Therefore, narrow size distribution is achieved in different layers after centrifugation.

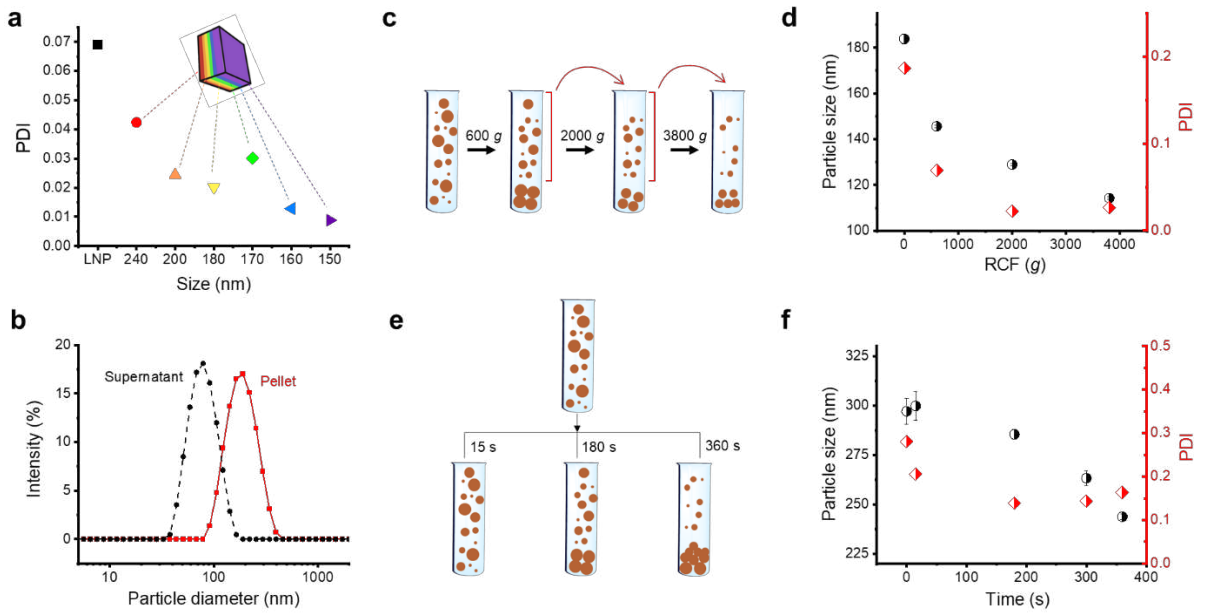

Figure 5. Mechanism study of size separation: centrifugation mechanism study through varying centrifugation force and time. (a) PDI of LNPs in different color layers after centrifugation. (b) DLS size distribution of LNPs in pellet and supernatant after centrifugation at 3800 × g for 2 h. (c) Scheme of differential centrifugation. (d) Size and PDI of supernatant after differential centrifugation with different RCF, first run with RCF of 600 × g, second 2000 × g and third 3800 × g. (e) Scheme of centrifugation for different time. (f) Size and PDI of supernatant after different centrifugation time.

We assume that rearrangement of particle assemblies can occur as long as there is a driving force. For easier observation we prepared LNPs with hydrodynamic size of 582 nm (SI Fig. S1) and studied their dynamic assembly during evaporation by *in situ* microscopic observation (SI video). As shown in Fig. 6a, chronicled screenshots from the video recording reveal how particles form a packed structure. The growth front[33], that is, from wet to dry regime, is shown by a black dot curve at the right bottom corner of the first image (0 s). Initially (0 s), a single particle which is pointed by a yellow arrow was brought to the edge of the evaporation front by capillary forces. This movement of the particle induces an

unbalanced force to the particles which exist at the growth front. As shown in the images at 0.23 s and 0.81 s, another particle which is pointed by red arrow started to move from its original position and at the end the particles formed a more packed structure, as shown by a yellow dot line in the image of 0.81 s. Similar phenomenon was also observed from 1.57 to 7.30 s. As pointed by a green arrow, a particle dynamically rearranged from its original position to a new position. At the end, a packed structure formed, as shown with a yellow dot line in the image recorded at 7.30 s. These observations explain the self-assembly of LNPs to form rectangular platelets in Fig. 2c and d.

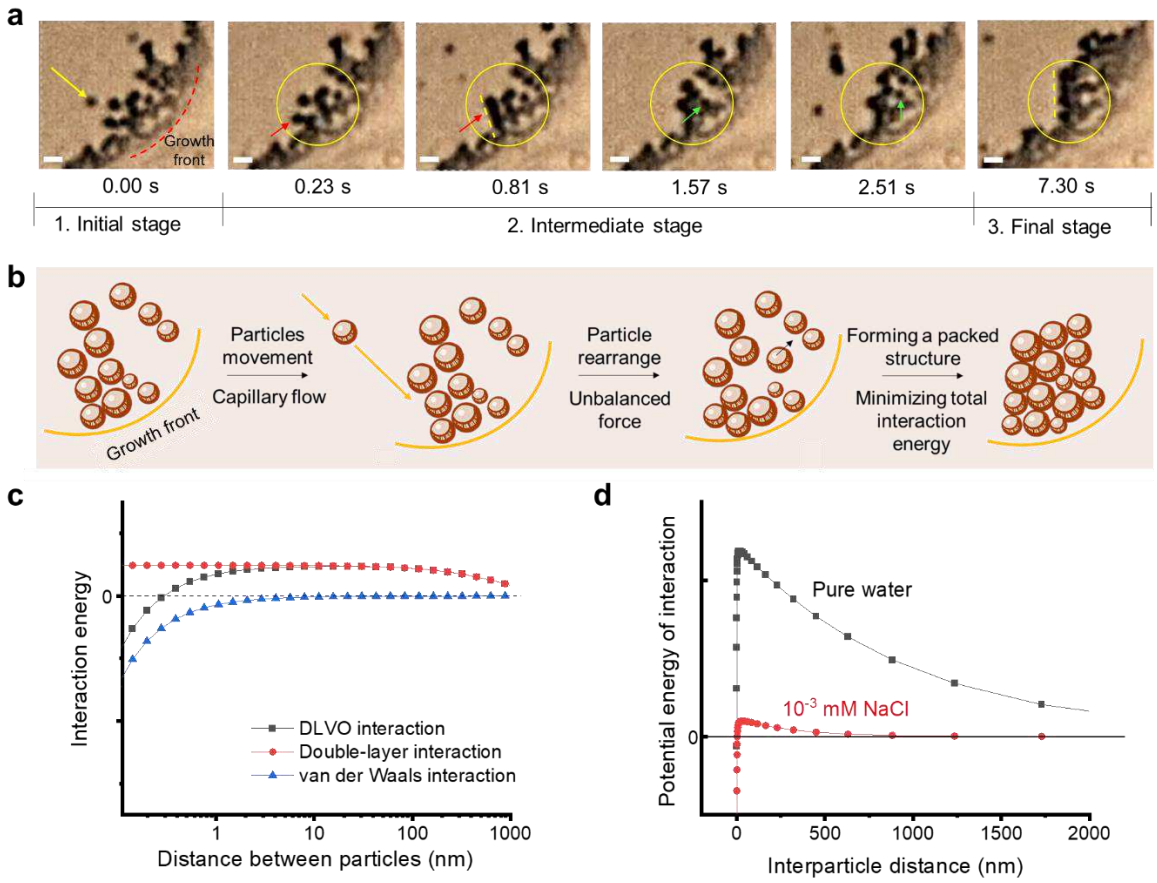

Figure 6. Dynamic analysis of particle assembly and interactions. (a) *M*icroscopy images from video recording captured during evaporation-induced self-assembly. The growth front is shown by a red dashed line. Scale bar 2 μm. Red and green arrows indicate two particles and how they rearrange. (b) Schematic illustration of the formation of a packed structure via rearrangement of particles. (c) Calculations of interactions (repulsive double-layer interaction, attractive van der Waals interaction, and DLVO interaction) in LNPs colloidal system by using DLVO model. (d) Calculations of DLVO interaction of LNPs particles in pure water and in salt solution.

For self-assembly to occur, a balanced combination of driving forces and colloidal forces is necessary[8]. Our *in situ* observation provides a testimony that particles experience three stages during rearrangement and that their assembly is driven by minimization of total interaction energy. At the initial stage, particles were brought to the edge of the evaporation front via capillary-induced water flow[33–35]. The movement of new incoming particles brings an unbalance force to the existing particles which are already at the growth front, therefore these particles rearrange to find another position where they are force-balanced. We call this step the intermediate stage. The DLVO theory[29] which describes the interaction forces between charged particles can explain the unbalanced force (Fig. 6c and d). As shown in Fig 6d, there is a peak in the DLVO potential when two particles are brought near, for example, from 1 μm to 10 nm. This strong repulsive peak is due to the charged surface of LNPs and the long Debye screening length in a low ion concentration in aqueous solution (Fig. 6d). At the final stage, particles rearrange until they form sufficiently large packed structures. This forming process is driven by minimizing total interaction energy[36].

Discussion

We have elucidated differences between evaporation-induced and centrifugation-assisted sedimentation of lignin nanoparticles into packed structures. Rectangular platelets resulted from evaporation under ambient conditions while photonic crystals appeared upon centrifugation. The relation between the particle size and observed structural color was derived from a modified Bragg's equation. Microscopic investigation revealed the ordered packing of lignin nanoparticles in the photonic layers that displayed a gradient from violet to red as observed by naked eyes and confirmed by reflection spectra in the visible wavelength range. Centrifugation has several key contributions to the structure formation. It removes small particles which disturb the photonic structures, increases the solid content of the pellet, and classifies the particles and increases monodispersity in each sedimented layer. Within the photonic layers, the particles were highly monodispersed (PDI < 0.05) and classified according to their physical size ranging from 150 nm to 240 nm. The *in situ* microscopy images provided additional insight into the dynamic rearrangement, assembly and interparticle interactions of lignin nanoparticles. We conclude that formation of photonic, close-packed ordered structures can be achieved by centrifugation-

assisted assembly of lignin nanoparticles, which opens new avenues towards advanced functional materials from these abundant and low-cost building blocks.

Methods

Materials and chemicals

All prepared lignin materials (LNPs and LNPs photonic crystal) in this work were prepared from soda lignin (PROTOBIND 2400, GreenValue LLC, previously characterized by ^{31}P NMR spectroscopy [30]). Ethanol (95%) from Kiilto, Sweden, and acetone (99.5%) from Honeywell, Germany were used as solvents in the fractionation procedure. Deionized (DI) water was used in all experiments.

Fractionation of soda lignin

Lignin was first purified with ethanol, and then was extract with acetone, according to a method reported in the literature[26]. Specifically, 50 g soda lignin was added to 400 mL ethanol under 600 rpm string for 30 min. The solid part of the lignin suspension was collected by centrifugation (3800 g, 10 min) and the solution part was removed. 300 g acetone was added to the solid part lignin and then string under 600 rpm for 1 h. The suspension was filtrated and the fractionated solution was used for preparing LNPs for next step.

Preparation of lignin nanoparticles (LNPs)

LNPs was prepared by similar solvent shifting method from literature[30]. The fractionated lignin solution (solid content: ~ 5 g) was added to 100 g DI water and stir under 600 rpm for 1 h. Then 1200 mL water was added to the solution (acetone/water, 3/1, w/w) with a water dilution rate of 20 v/v/min, LNPs size was around 190 nm, the final LNP dispersion was 0.18 wt%. Another two different size LNPs (316 nm and 582 nm) were prepared by varying water dilution rate to 3 and 0.25 v/v/min respectively.

Evaporation-driven assembly of LNPs into platelets

Strip pattern was prepared by evaporation-induced assembly of LNPs. 3 mL LNPs dispersion was added to a Petri dish (diameter: 3.5 cm). The pattern was formed after solvent evaporation.

Preparation of LNPs photonic crystal

LNPs photonic crystal was prepared by centrifugation (Sorvall LYNX 6000 Superspeed Centrifuge). Specifically, 200 mL LNPs dispersion (size: ~ 190 nm) was added to 500 mL centrifuge bottle and centrifuged at force of 3800 × g for 2 h. The supernatant was carefully removed and the pellet was dried under room temperature.

Characterization

Dynamic light scattering

A Zetasizer Nano ZS (Malvern, UK) was used to measure the size distribution of LNPs by dynamic light scattering (DLS). 20 μL of LNPs dispersion was added to 2 mL DI water. The diluted LNPs dispersion samples were measured 3 times with 12 runs per run. Median values were reported.

UV–Vis spectrophotometry

A UV–Vis spectrophotometer (Agilent Cary 5000 UV–Vis–NIR) was used to measure the optical properties of LNPs photonic crystal in visible range. The reflectance spectrums of LNPs photonic crystal were recorded with the praying mantis diffuse reflectance accessory in the range of 350–800 nm with a specialized fluorine-based polymer as reference.

Microscopy

A JSM-7401F field emission scanning electron microscope was used to image LNPs and LNPs photonic crystal samples. An accelerating voltage of 1-2 kV and working distance of 2-15 mm was used during measurement. Some samples were coated for 60-120 s with gold using a JFC-1200 fine coater before the SEM study. The gold particles added by sputtering are about 5 to 15 nm in size and they were added to increase the contrast in the images. Annular dark field (ADF) scanning transmission electron microscopy (STEM) images were obtained using a ThermoFisher Themis Z double aberration-corrected

TEM operated at 300 kV with a convergence angle of 21 mrad and a dwell time of 3 µs. The material was sectioned to 200 nm thickness using ultramicrotomy using a Leica Ultracut UCT with a 45° diamond knife (Diatome, Czech Republic) after the crystalline lignin nanoparticles first had been embedded in Agar low viscosity resin to facilitate sectioning.

A Nikon FN-S2N (Japan) microscope was used to image the rectangular platelets of LNPs and record a video of the assembly and rearrangement of LNPs during evaporation. A Dino-Lite Edge3.0 digital microscope was used to image photonic crystals of LNPs.

Calculation of particle size − wavelength relationship

The particle size which responds to different visible wavelength scales (at normal incidence) can be predicted from the diffraction of electromagnetic waves following a modified Bragg's law[7,28,29]. equation (1),

$$\lambda = 2n_{eff}\, d_{111} \tag{1}$$

where n_{eff} is the effective refractive index of lignin, d_{111} is the interplanar spacing within the (111) plane, the latter dependent on *D* which is the particle diameter (unit: nm), for an array of cubic close-packed spheres, and under assumption that particles are rigid and touching, the relationship between the sphere radius and the spacing of the (111) planes is:

$$d_{111} = \sqrt{\frac{2}{3}} D \tag{2}$$

the n_{eff} can be calculated by using following equation:

$$n_{eff} = \sqrt{\varphi n_{lig} + (1-\varphi) n_{air}} \tag{3}$$

n_{lig} and n_{air} are refractive indices of lignin and air, 1.61[37] and 1, respectively, and φ is the volume fraction of particles in a close packing, which is 0.7405.

Interparticle force calculations based on the DLVO theory

Repulsive double-layer interaction $V(D)_{DL}$ can be calculated by equation (4),[29]:

$$V(D)_{DL} = \frac{64\pi RkTn(\infty)}{\kappa}\tanh^2\left(\frac{z\phi_0}{4kT}\right)\exp(-\kappa D) \quad (4)$$

where R is particle size (≈ 500 nm), k is Boltzmann constant (= 1.38× 10^{-23} J/K), T is absolute temperature (= 300 K), $n(\infty)$ is number density of ions in bulk solution (for pure water, = 6.022× 10^{19} ions/m^3), z is ion valency (for pure water, = 1), ϕ_0 is surface potential (≈ −37 mV [30]), D is the distance between particles. κ^{-1} is Debye-length, which can be calculated by:

$$\kappa^{-1} = \sqrt{\frac{kT\varepsilon_0\varepsilon_r}{2e^2z^2n(\infty)}} \quad (5)$$

where ε_0 is permittivity of vacuum (= 8.854×10^{-12} F/m), ε_r is relative dielectric constant (= 78.5 F/m), e is elementary charge (=1.6 × 10^{-19}).

Attractive van der Waals interaction $V(D)_{vdW}$ can be calculated by:

$$V(D)_{vdW} = -\frac{AR}{12D} \quad (6)$$

where A is Hamaker constant (= 1.7× 10^{-20} J [38]). The force is always attractive between two identical materials across a medium.

Therefore, DLVO interaction $V(D)_{DLVO}$ can be calculated by:

$$V(D)_{DLVO} = V(R) + V(A) \quad (7)$$

References

1. Ling, Z. et al. Nature-inspired construction of iridescent CNC/Nano-lignin films for UV resistance and ultra-fast humidity response. Carbohydr. Polym. 296, 119920 (2022).
2. Chu, G., et al. Self-assembled nanorods and microspheres for functional photonics: retroreflector meets microlens array. Adv. Opt. Mater 9, 2002258 (2021).
3. Yin, H. *et al.* Amorphous diamond-structured photonic crystal in the feather barbs of the scarlet macaw. *Proc. Natl Acad. Sci. USA* **109**, 10798–10801 (2012).
4. Doekele, G. S., Hein, L. L., Daniel, C. O. & Bodo, D. W. High refractive index of melanin in shiny occipital feathers of a bird of paradise. *Light Sci. Appl.* **4**, 1–6 (2015).
5. Cai, Z. *et al.* From colloidal particles to photonic crystals: advances in self-assembly and their

emerging applications. *Chem. Soc. Rev.* **50**, 5898–5951 (2021).

6. Meijer, J. M. *et al.* Self-assembly of colloidal cubes via vertical deposition. *Langmuir* **28**, 7631–7638 (2012).

7. Gao, W., Rigout, M. & Owens, H. Self-assembly of silica colloidal crystal thin films with tuneable structural colours over a wide visible spectrum. *Appl. Surf. Sci.* **380**, 12–15 (2016).

8. Armstrong, E. & O'Dwyer, C. Artificial opal photonic crystals and inverse opal structures-fundamentals and applications from optics to energy storage. *J. Mater. Chem. C* **3**, 6109–6143 (2015).

9. Armstrong, E. *et al*. Ordered 2D colloidal photonic crystals on gold substrates by surfactant-assisted fast-rate dip coating. *Small* **10**, 1895-1901 (2014).

10. Jiang, P., Bertone, J. F., Hwang, K. S. & Colvin, V. L. Single-crystal colloidal multilayers of controlled thickness. *Chem. Mater.* **11**, 2132–2140 (1999).

11. Rogach, A. L., Kotov, N. A., Koktysh, D. S., Ostrander, J. W. & Ragoisha, G. A. Electrophoretic deposition of latex-based 3D colloidal photonic crystals: A technique for rapid production of high-quality opals. *Chem. Mater.* **12**, 2721–2726 (2000).

12. Chen, Y., Zhang, C., Zheng, Q. & Chen, Y. Separation-cooperated assembly of liquid photonic crystals from polydisperse particles. *Chem. Commun.* **54**, 13937–13940 (2018).

13. Pusey, P. N. & van Megen, W. Phase behaviour of concentrated suspensions of nearly colloidal spheres. *Nature* 2–4 (1986).

14. Wu, Y. *et al.* Preparation and application of photonic crystal paints with tunable structural colors. *Phys. Status Solidi Appl. Mater. Sci.* **217**, 1–10 (2020).

15. Si, M. *et al.* Phase separation of co-solvent promotes multiple bio-nanomaterials conversion from natural lignocellulose. *Ind. Crops Prod.* **152**, 112469 (2020).

16. Zhang, H., Fu, S. & Chen, Y. Basic understanding of the color distinction of lignin and the proper selection of lignin in color-depended utilizations. *Int. J. Biol. Macromol.* **147**, 607–615 (2020).

17. Wang, J. *et al.* Reduction of lignin color via one-step UV irradiation. *Green Chem.* **18**, 695–699 (2016).

18. Gierer, J. Chemistry of delignification. *Wood Sci. Technol.* **19**, 289–312 (1986).

19. Sipponen, M. H., Lange, H., Ago, M. & Crestini, C. Understanding lignin aggregation processes. A case study: budesonide entrapment and stimuli controlled release from lignin nanoparticles. *ACS Sustain. Chem. Eng.* **6**, 9342–9351 (2018).

20. Conner, C. G., Veleva, A. N., Paunov, V. N., Stoyanov, S. D. & Velev, O. D. Scalable formation of concentrated monodisperse lignin nanoparticles by recirculation-enhanced flash nanoprecipitation. *Part. Part. Syst. Charact.* **37**, 1–10 (2020).

21. Rodrigues, J. S., Lima, V., Araújo, L. C. P. & Botaro, V. R. Lignin fractionation methods: can lignin fractions be separated in a true industrial process? *Ind. Eng. Chem. Res.* **60**, 10863–10881 (2021).

22. Zhao, W., Simmons, B., Singh, S., Ragauskas, A. & Cheng, G. From lignin association to nano-/micro-particle preparation: Extracting higher value of lignin. *Green Chem.* **18**, 5693–5700 (2016).

23. Sadeghifar, H. *et al.* Perspective on technical lignin fractionation. *ACS Sustain. Chem. Eng.* **8**, 8086–8101 (2020).

24. Majdar, R. E., Crestini, C. & Lange, H. Lignin fractionation in segmented continuous flow. *ChemSusChem* **13**, 4735–4742 (2020).

25. Moreno, A. & Sipponen, M. H. Biocatalytic nanoparticles for the stabilization of degassed single electron transfer-living radical pickering emulsion polymerizations. *Nat. Commun.* **11**, 5599 (2020).

26. Wang, J. *et al.* Monodispersed lignin colloidal spheres with tailorable sizes for bio-photonic materials. *Small* **18**, 2200671, (2022).

27. Vukusic, P. & Sambles, J. R. Photonic Structures in biology. *Nature* **424**, 852–855 (2003).

28. Tilley, R. J. D. *Colour and the Optical Properties of Materials: An Exploration of the Relationship Between Light, the Optical Properties of Materials and Colour*. (John Wiley & Sons, 2011).

29. Ng, E. C. H., Koh, Y. K. & Wong, C. C. *Colloidal crystals.* (Contemporary Physics*,* 2012).

30. Liu, J. *et al.* Fully biobased photothermal films and coatings for indoor ultraviolet radiation and heat management. *ACS Appl. Mater. Interfaces* **14**, 12693–12702 (2022).

31. Cusola, O. *et al.* Particulate coatings via evaporation-induced self-assembly of polydisperse colloidal lignin on solid interfaces. *Langmuir* **34**, 5759–5771 (2018).

32. Jiang, P., Bertone, J. F. & Colvin, V. L. A lost-wax approach to monodisperse colloids and their crystals. *Science* **291**, 453–457 (2001).

33. Suh, Y., Gowda, H. & Won, Y. In situ investigation of particle clustering dynamics in colloidal assemblies using fluorescence microscopy. *J. Colloid Interface Sci.* **576**, 195–202 (2020).

34. Deegan, R. D., *et al.* Capillary flow as the cause of ring stains from dried liquid drops *Nature* **389** 827–829 (1997).

35. Velev, O. D. *et al.* Mechanism of formation of two-dimensional crystals from latex particles on substrata. *Prog. Colloid Polym. Sci.* **93**, 366–367 (1993).

36. Serpe, M. J., Kang, Y. & Zhang, Q. M. *Photonic materials for sensing, biosensing and display devices*. (Springer Series in Materials Science, 2015).

37. Li, Y., Fu, Q., Yu, S., Yan, M. & Berglund, L. Optically transparent wood from a nanoporous cellulosic template: combining functional and structural performance. *Biomacromolecules* **17**, 1358–1364 (2016).

38. Hollertz, R. *et al.* Dielectric properties of lignin and glucomannan as determined by spectroscopic ellipsometry and Lifshitz estimates of non-retarded Hamaker constants. *Cellulose* **20**, 1639–1648 (2013).

Supplementary Files

This is a list of supplementary files associated with this preprint. Click to download.

- SI.pdf
- SupplementaryVideo.mp4